Materials Advances

ROYAL SOCIETY OF CHEMISTRY

PAPER

View Article Online
View Journal | View Issue

Cite this: *Mater. Adv.*, 2024, 5, 8233

Received 7th August 2024,
Accepted 22nd September 2024

DOI: 10.1039/d4ma00796d

rsc.li/materials-advances

Revealing uranium tetrafluoride microrods†

Harry Jang and Frederic Poineau *

Anhydrous and hydrated UF_4 microrods (5–25 μm) were prepared from the reactions of UO_2 microrods (5–15 μm) with HF(g), produced from the decomposition of silver bifluoride ($AgHF_2$, SBF). In order to optimize the preparation of UF_4 mr, several experimental parameters including atmosphere (air or N_2), temperature (150 or 250 °C) and amount of SBF were evaluated. In all reactions, rodlike morphologies were retained. At 250 °C, the reaction products always consist of an anhydrous UF_4/hydrated UF_4 mixture, while at 150 °C only hydrated UF_4 was detected. Anhydrous UF_4 microrods were obtained by dehydration of the anhydrous UF_4/hydated UF_4 mixture using TGA-DSC. Changing the atmosphere from air to N_2 or reducing the amount of SBF by half did not affect the nature of the reaction products.

Introduction

At the nano- and microscale, materials can exhibit properties (*e.g.*, optical, catalytic, electronic, mechanical, thermal, magnetic)[1–3] that are not observed at the macroscale. The common applications of micro- and nano- materials (*e.g.* gas sensors, electrochromic devices, solar cells, batteries) are shared between many metal oxides (*e.g.* Ti,[4] Co,[1,5,6] Ni,[2,7] Zn,[8–10] Mo,[11–15] and In[16,17]). The rod-morphology is one of the most studied and examples of microrods and nanorods respectively include $In_{1-x}Ga_xP$,[18] MnOOH,[19] Bi_2S_3,[20] and Ga_2O_3.[21]

One element whose material chemistry of micro- and nanorods has been poorly studied is uranium. Research on uranium has primarily focused on the study of spherical particles of binary oxides, nitrides, carbides, and fluorides.[22–28] Uranium microstructures can find applications as targets for medical isotope production,[29–31] fuels for nuclear reactors,[32–34] standards for nuclear forensics,[35–37] and energy sources for space exploration.[38] Morphological studies of uranium materials are also relevant to the field of nuclear forensics.[39,40] One critical material for the nuclear industry is UF_4, which is produced from the reaction of UO_2 with HF gas at elevated temperatures (eqn (1)).

$$UO_2(s) + 4HF(g) \rightarrow UF_4(s) + 2H_2O(g) \quad (1)$$

Besides serving as an intermediate in UF_6 production,[41,42] UF_4 has also found applications as targets for heavy ion production[43] and the primary precursor material for U metal production.[44] It is also proposed as a fuel for molten salt reactors.[45] Anhydrous UF_4, a green solid with low solubility in water,[46] exhibits several hydrated forms (*i.e.*, $UF_4{\cdot}xH_2O$, x = 0.5, 0.7, 0.75, 1.2, 1.3, 1.5, 2.0, 2.5)[47–49] which are formed upon reactions of the material with water (eqn (2)).

$$UF_4(s) + xH_2O(g) \rightarrow UF_4{\cdot}xH_2O(s) \quad (2)$$

As water is ubiquitous in the uranium industry, it is important to address environmental and industrial concerns pertaining to the hydrolytic behaviors of UF_4.[48] Though the physico-chemical properties of UF_4 and its hydrates are well characterized at the macroscale,[47–64] there is a lack of knowledge concerning their preparations and characterizations at the microscale. As the applications of UF_4 expand, it is essential that information and accessibility to UF_4 materials at the microscale become more readily available.

So far, the only UF_4 morphology that can be prepared and controlled at the microscale is the spherical one. UF_4 microspheres (ms) have already been produced and are commercially available,[27,49,54,65] and although details on their production remain proprietary, high temperature hydrofluorination of UO_2 was mentioned.[66] Other UF_4 morphologies such as microrods (mr) or microplates (mp) have not yet been prepared in a controlled manner.

Previously, we have reported on the preparation of UO_2F_2 microspheres, microrods and microplates using chemical transformation.[28,67] In these works, uranium oxide micromaterials (UO_3, U_3O_8) were fluorinated in an autoclave with HF(g) produced from the thermal decomposition of silver bifluoride ($AgHF_2$, SBF). Scanning electron microscope (SEM) results concerning the morphology and particle size distribution of UO_2F_2 mp have shown high variance, whereas SEM results relating to UO_2F_2 mr have been consistent. As a continuation, investigating U(IV) fluoride micromaterials was a natural

Department of Chemistry & Biochemistry, University of Nevada, Las Vegas, Las Vegas, Nevada 89154, USA. E-mail: poineauf@unlv.nevada.edu

† Electronic supplementary information (ESI) available. See DOI: https://doi.org/10.1039/d4ma00796d

progression and microrods were selected as the primary microstructure.

Here, we report on the preparation of anhydrous and hydrated UF_4 microrods. The materials were prepared by chemical transformation from the reaction of UO_2 mr with SBF in autoclaves and were characterized by scanning electron microscopy and powder X-ray diffraction (PXRD).

Experimental

Caution! Uranium-238 is an α emitter (E_{max} = 4.26 MeV). All manipulations were performed in a designed radiochemistry laboratory equipped with HEPA filter hoods and by following approved radioisotope handling and monitoring procedures.

Materials and methods

Silver bifluoride (≥99%, Alfa Aesar), glycerol (≥99.5%, Sigma-Aldrich), and urea (≥98%, Sigma-Aldrich) were used as received. $UO_2(NO_3)_2{\cdot}6H_2O$ (UNH) was prepared from the treatment of uranium metal dissolved in hot nitric acid followed by recrystallization. Fluorination and hydrothermal reactions were conducted within a Parr model 4749 autoclave placed in a Thermo Scientific Thermolyne Benchtop muffle furnace (model FB1315M). Fluorinations were conducted at 150–250 °C for 6–24 hours in the setup reported previously.[67] For dry reactions, N_2 was regarded as inert as it does not react with reactants at these temperatures. HF(g), the gaseous decomposition product of SBF, provides the source of fluorine for the reactions. In these reactions, SBF in excess molar quantity was placed on the Teflon liner of the vessel, while the uranium oxide material was placed in a 15 mL Teflon vial above the SBF.[67]

Powder X-ray diffraction measurements were performed at room temperature on a Bruker D8 Advanced diffractometer equipped with Cu Kα X-rays (λ = 1.5406 Å) and a solid-state Si detector. Imaging was performed on the JEOL Tescan CLARA field emission scanning electron microscope, and samples were mounted on carbon tape without coating. TGA-DSC measurements were conducted with a TA instruments SDT 650 Discovery series TGA-DSC from 50–600 °C with a heating rate of 10 °C min^{-1}. The measurements were performed in alumina crucibles under flowing argon gas with a sample and balance flow rate of approximately 100 mL min^{-1}. Particle sizes were measured using ImageJ, and particle size distribution figures were generated using SciDAVis.

Sample preparation

Preparation of UO_2 mr. $3UO_3{\cdot}NH_3{\cdot}5H_2O$ mr (234.1 mg, 0.244 mmol), prepared using the reported method,[68] was placed in an alumina boat and treated at 600 °C for 3 hours under air. The resulting U_3O_8 product (172.3 mg, 0.205 mmol) was then heated to 600 °C for 5 hours under flowing 5% H_2/95% Ar gas.[69] The resulting UO_2 mr (159 mg, 0.589 mmol, 80.6% yield from $3UO_3{\cdot}NH_3{\cdot}5H_2O$) was characterized by SEM (Fig. 1) and PXRD (Fig. S1, ESI†) (Table 1).

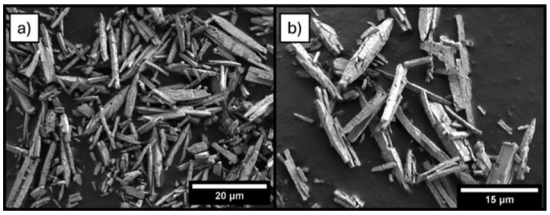

Fig. 1 SEM images of UO_2 mr at (a) 4790× and (b) 6640×.

Results and discussion

Here, the reactions were set up identically to previous UO_2F_2 microrod works except that the starting material (*i.e.*, U_3O_8 mr) was replaced with UO_2 mr.

Various experimental parameters have been evaluated (atmosphere, temperature, amount of SBF). A total of four reactions were investigated. In each reaction, UO_2 was weighed and placed in a Teflon vial and then placed in the Teflon liner of the autoclave containing SBF. The autoclave was sealed either in air (reaction 1, 3, and 4) or under N_2 atmosphere (reaction 2) and thermally treated for 24 hours at 150 or 250 °C. Following the reaction, the autoclave was cooled for 2 hours to room temperature and opened, and the resulting product was weighed and characterized by PXRD and SEM. The conditions, reaction products, and yields for the four reactions are presented in Table 1, and the effects of atmosphere, temperature, and amount of SBF on the nature of the reaction products are discussed in the following sections.

Baseline reaction

Reaction 1 follows the same procedure as the one applied for the preparation of UO_2F_2 (24 hours at 250 °C using ∼300 mg SBF [U:HF = ∼3–5] prepared in air). Here the reaction of UO_2 and HF(*g*) led to a mixture of anhydrous and hydrated UF_4 (Fig. S2a, ESI†). The presence of hydrated UF_4 in the reaction product is probably due to the reaction of UF_4 and water (eqn (2)) that was formed as a byproduct (eqn (1)).

Morphologically, the rodlike particles remained intact and experienced some visible surface roughing (Fig. 2a–c). Particle

Table 1 Experimental conditions and reaction products for the fluorination of UO_2 mr with SBF

Reaction #	Mass of UO_2 (mg)	Mass of SBF (mg)	T (°C)	Time (h)	Atmosphere	Yield (mg, %)	Reaction product
1	50.8	303.9	250	24	Air	57.9 (98.0%)	$UF_4/UF_4{\cdot}2H_2O$
2	30.1	400.0	250	24	N_2	29.5 (82.3%)	$UF_4/UF_4{\cdot}xH_2O$
3	31.5	301.6	150	24	Air	35.0 (86.0%)	$UF_4{\cdot}1.5H_2O$
4	33.8	155.8	250	24	Air	35.2 (89.6%)	$UF_4/UF_4{\cdot}2H_2O$

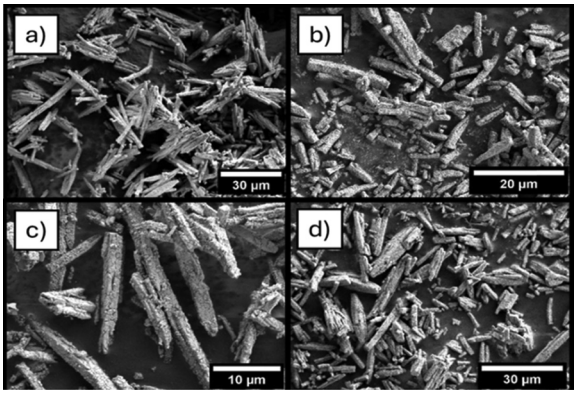

Fig. 2 SEM images of the reaction products of reaction 1 at (a) 2000×, (b) 4450×, (c) 6650×, and (d) after TGA-DSC at 2650×.

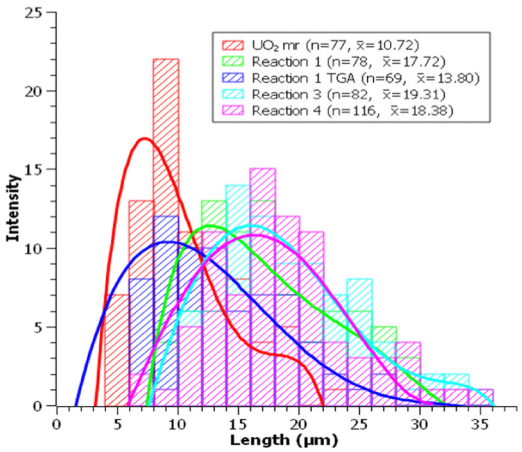

Fig. 3 Particle size distribution of UO_2 mr and particles from reaction 1, 3, and 4.

size distribution (PSD) analysis (Fig. 3) shows the average length of these particles have increased by ~7 μm.

Treatment of the reaction product (16.94 mg) by TGA-DSC up to 600 °C (ramp rate of 10 °C min^{-1}) under argon converted the $UF_4/UF_4{\cdot}2H_2O$ mixture to anhydrous UF_4. The TGA-DSC curves (Fig. S3, ESI†) show a steady mass decrease followed by a plateau at ~380 °C, indicating the point of complete dehydration to anhydrous UF_4. Following TGA-DSC, the sample was characterized by SEM (Fig. 2d) and PXRD (Fig. S2b, ESI†). SEM

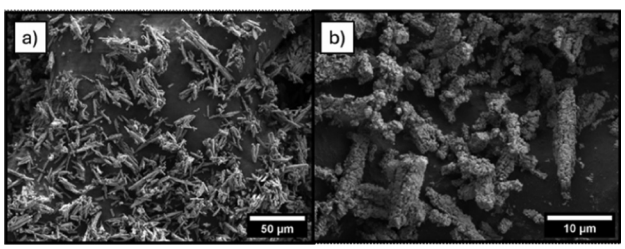

Fig. 4 SEM images of the reaction products of reaction 2 at (a) 1260× and (b) 7360×.

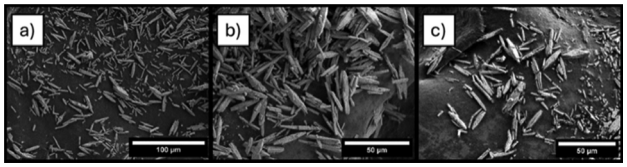

Fig. 5 SEM images of the reaction products of reaction 3 at (a) 1950× and (b) 3510×, and reaction 4 at (c) 3080×.

analysis shows no morphological changes to the particles, and PSD analysis showed a decrease in average particle length by ~4 μm. The dehydration of UF_4/UF_4 hydrate proved efficient for the preparation of anhydrous UF_4 mr and could be transposed to other morphologies of UF_4 hydrates.

Effect of atmosphere

The effect of atmosphere on the reaction product was investigated in reaction 2. Treatment of UO_2 with HF(g) under N_2 atmosphere at 250 °C for 24 hours yielded a mixture of anhydrous UF_4 and hydrated UF_4 (PXRD in Fig. S2c, ESI†). SEM shows the rods to exhibit rough surfaces that were not observed in the UO_2 mr precursor (Fig. 4), and PXRD shows less hydrated UF_4 than from the one from reaction 1 (Fig. S2c, ESI†).

Effect of temperature

Reaction 3 was performed at 150 °C, while the other parameters (atmosphere, reaction time, and amount of SBF) were identical to the baseline reaction. Following the reaction, PXRD analysis (Fig. S2d, ESI†) shows the presence of $UF_4{\cdot}1.5H_2O$ as a single phase.

SEM analysis (Fig. 5a and b) shows the $UF_4{\cdot}1.5H_2O$ mr to exhibit smoother surfaces than the reaction products from reactions 1 and 2. The particle size distributions (Fig. 3) showed no size disparities between $UF_4{\cdot}1.5H_2O$ mr and that of $UF_4/UF_4{\cdot}2H_2O$ mr (reaction 1).

The absence of anhydrous UF_4 at 150 °C indicated that the hydrate was initially formed near this temperature and that the increase in temperature to 250 °C would initiate dehydration leading to the partially hydrated mixture. We hypothesized that the reaction at 400 °C should lead exclusively to anhydrous UF_4.

Effect of SBF

In reaction 4, about half the amount of $AgHF_2$ was used (155.8 mg, 1.061 mmol). Calculations indicated that at 250 °C, decreasing the amount of SBF by half would decrease the partial pressure of HF(g) in the autoclave from ~4 atm to ~2 atm (~5 atm to ~3 atm total pressure). PXRD analysis showed the presence of a $UF_4/UF_4{\cdot}2H_2O$ mixture (Fig. S2e, ESI†) while SEM (Fig. 5c) indicated the presence of microrods. PSD observations (Fig. 4) were consistent with the results of reactions 1 and 3. Overall, decreasing the amount of SBF does not fundamentally change the nature of the reaction products as anhydrous UF_4 and hydrated UF_4 were obtained.

Conclusions

For the first time, uranium tetrafluoride microrods were prepared by chemical transformation. The reactions of UO_2 microrods (5–15 μm) with HF(g), produced from the decomposition of SBF, were investigated in autoclaves. Several experimental parameters including atmosphere, temperature, and amount of SBF were tested. In all reactions, rodlike morphologies were retained. At 250 °C, the reaction products always consist of an anhydrous UF_4/hydrated UF_4 mixture, while at 150 °C only the presence of hydrated UF_4 was detected. Anhydrous UF_4 microrods were obtained by dehydration of the anhydrous UF_4/hydrated UF_4 mixture *via* thermal treatment using TGA-DSC. Changing the atmosphere from air to N_2 or reducing the amount of SBF by half did not fundamentally affect the nature of the reaction products. Using experimental set-up to 250 °C for the highest operational temperature indicated that the preparation of single phase hydrated UF_4 or anhydrous UF_4 is respectively a one-step (hydrofluorination) and two-step process (hydrofluorination and dehydration). The preparation of anhydrous UF_4 in a single step process would require hydrofluorination in an autoclave at $T > 250$ °C.

Currently, the preparation of UF_4 nanospheres and microplates using the method presented here is under progress and results will be reported in due course. Finally, successful fluorinations of uranium oxide micromaterials will lay the groundwork for the development of other f-element fluoride micromaterials.

Author contributions

The manuscript was written through contributions of all authors. H. J.: investigation, methodology, validation, visualization, and writing – original draft. F. P.: conceptualization, funding acquisition, project administration, resources, supervision, and writing – review & editing.

Data availability

The data supporting this article have been included as part of the ESI.†

Conflicts of interest

There are no conflicts to declare.

Acknowledgements

This material is based upon work performed under the auspices of the Consortium on Nuclear Security Technologies (CONNECT) supported by the Department of Energy/National Nuclear Security Administration under Award Number(s) DE-NA0003948. The authors would like to thank Mrs Wendee Johns for administrative support and Mr Quinn Summerfield for laboratory support.

References

1 S. Iravani and R. S. Varma, *Green Chem.*, 2020, **22**, 2643–2661.
2 M. Imran Din and A. Rani, *Int. J. Anal. Chem.*, 2016, **2016**, 1–14.
3 M. A. Albrecht, C. W. Evans and C. L. Raston, *Green Chem.*, 2006, **8**, 417–432.
4 V. K. H. Bui, V. Van Tran, J. Y. Moon, D. Park and Y. C. Lee, *Nanomaterials*, 2020, **10**, 1–31.
5 D. Alburquenque, E. Vargas, J. C. Denardin, J. Escrig, J. F. Marco, J. Ortiz and J. L. Gautier, *Mater. Charact.*, 2014, **93**, 191–197.
6 N. Wu, J. Shen, L. Sun, M. Yuan, Y. Shao, J. Ma, G. Liu, D. Guo, X. Liu and Y. B. He, *Electrochim. Acta*, 2019, **310**, 70–77.
7 S. S. Narender, V. V. S. Varma, C. S. Srikar, J. Ruchitha, P. A. Varma and B. V. S. Praveen, *Chem. Eng. Technol.*, 2022, **45**, 397–409.
8 J. H. Kim, D. Andeen and F. F. Lange, *Adv. Mater.*, 2006, **18**, 2453–2457.
9 T. Gao and T. H. Wang, *Appl. Phys. A: Mater. Sci. Process.*, 2005, **80**, 1451–1454.
10 Q. Deng, X. Duan, D. H. L. Ng, H. Tang, Y. Yang, M. Kong, Z. Wu, W. Cai and G. Wang, *ACS Appl. Mater. Interfaces*, 2012, **4**, 6030–6037.
11 X. Hu, W. Zhang, X. Liu, Y. Mei and Y. Huang, *Chem. Soc. Rev.*, 2015, **44**, 2376–2404.
12 J. Sun, Y. Dong, X. Wang, J. Cao, M. Gong and C. Li, *J. New Mater. Electrochem. Syst.*, 2021, **24**, 73–77.
13 J. Zhou, N. S. Xu, S. Z. Deng, J. Chen, J. C. She and Z. L. Wang, *Adv. Mater.*, 2003, **15**, 1835–1840.
14 T. S. Sian and G. B. Reddy, *J. Appl. Phys.*, 2005, **98**, 6104.
15 C. D. A. Lima, J. V. B. Moura, G. S. Pinheiro, J. F. D. F. Araujo, S. B. S. Gusmão, B. C. Viana, P. T. C. Freire and C. Luz-Lima, *Ceram. Int.*, 2021, **47**, 27778–27788.
16 S. Luo, W. Zhou, W. Wang, Z. Zhang, L. Liu, X. Dou, J. Wang, X. Zhao, D. Liu, Y. Gao, L. Song, Y. Xiang, J. Zhou and S. Xie, *Appl. Phys. Lett.*, 2005, **87**, 3109.
17 J. Bartolomé, A. Cremades and J. Piqueras, *J. Mater. Chem. C*, 2013, **1**, 6790–6799.
18 M. K. K. Nakaema, M. P. F. Godoy, M. J. S. P. Brasil, F. Iikawa, D. Silva, M. Sacilotti, J. Decobert and G. Patriarche, *J. Appl. Phys.*, 2005, **98**, 3506.
19 Y. Zhang, Y. Liu, F. Guo, Y. Hu, X. Liu and Y. Qian, *Solid State Commun.*, 2005, **134**, 523–527.
20 G. Xie, Z.-P. Qiao, M.-H. Zeng, X.-M. Chen and S.-L. Gao, *Cryst. Growth Des.*, 2004, **4**, 513–516.
21 J. Zhang, Z. Liu, C. Lin and J. Lin, *J. Cryst. Growth*, 2005, **280**, 99–106.
22 J. H. Yang, Y. W. Rhee, D. Kim, J. H. Kim, K. W. Kang and K. S. Kim, *Transactions of the Korean Nuclear Society Autumn Meeting*, Gyeongju, Korea, 2006, pp. 1–2.
23 C. M. Silva, R. D. Hunt, L. L. Snead and K. A. Terrani, *Inorg. Chem.*, 2015, **54**, 293–298.
24 G. Ledergerber, Z. Kopajtic, F. Ingold and R. W. Stratton, *J. Nucl. Mater.*, 1992, **188**, 28–35.

25 T. B. Lindemer, S. L. Voit, C. M. Silva, T. M. Besmann and R. D. Hunt, *J. Nucl. Mater.*, 2014, **448**, 404–411.
26 W. Tian, H. Guo, D. Chen, M. A. Pouchon, A. Horwege, X. Yin, Q. Huang, J. Wang, S. Cao, D. Chen, J. Bai, C. Tan, F. Fan, X. Wu, T. Shen and Z. Qin, *Ceram. Int.*, 2018, **44**, 17945–17952.
27 B. J. Foley, J. H. Christian, C. A. Klug, E. Villa-Aleman, M. S. Wellons, M. DeVore, N. Groden and J. Darvin, *Dalton Trans.*, 2022, **51**, 6061–6067.
28 H. Jang, J. Louis-Jean and F. Poineau, *ACS Omega*, 2023, **8**, 21996–22002.
29 R. Henry and H. Saclay, *The use of recoil for the separation of uranium fission products; Utilisation du recul pour la separation des produits de fission de l'uranium*, France, 1959.
30 U. Passy and N. H. Steiger, *Nucl. Sci. Eng.*, 1963, **15**, 366–374.
31 J. M. Dorhout, M. P. Wilkerson and K. R. Czerwinski, *J. Radioanal. Nucl. Chem.*, 2019, **320**, 415–424.
32 L. R. Khanal, J. A. Sundararajan and Y. Qiang, *Energy Technol.*, 2020, **8**, 1–23.
33 E. A. Filippov, A. I. Karelin, O. P. Lobas, A. S. Papkov, A. N. Zhiganov, L. A. Mishina and V. I. Shamin, *J. Radioanal. Nucl. Chem.*, 1990, **143**, 53–60.
34 A. C. Robisson, S. Lemonnier and S. Granjean, *Atalante*, 2004, 1–4.
35 R. Middendorp, M. Dürr and D. Bosbach, *Procedia Chem.*, 2016, **21**, 285–292.
36 S. Richter, J. Truyens, C. Venchiarutti, Y. Aregbe, R. Middendorp, S. Neumeier, P. Kegler, M. Klinkenberg, M. Zoriy, G. Stadelmann, Z. Macsik, A. Koepf, M. Sturm, S. Konegger-Kappel, A. Venzin, L. Sangely and T. Tanpraphan, *J. Radioanal. Nucl. Chem.*, 2022, 1–5.
37 P. Kegler, F. Pointurier, J. Rothe, K. Dardenne, T. Vitova, A. Beck, S. Hammerich, S. Potts, A. L. Faure, M. Klinkenberg, F. Kreft, I. Niemeyer, D. Bosbach and S. Neumeier, *MRS Adv.*, 2021, **6**, 125–130.
38 W. J. Carmack, W. C. Richardson, D. L. Husser and T. C. Mohr, *AIP Conf. Proc.*, 2004, **699**, 420–425.
39 I. J. Schwerdt, C. G. Hawkins, B. Taylor, A. Brenkmann, S. Martinson and L. W. McDonald, *Radiochim. Acta*, 2019, **107**, 193–205.
40 L. W. McDonald, K. Sentz, A. Hagen, B. W. Chung, C. A. Nizinski, I. J. Schwerdt, A. Hanson, S. Donald, R. Clark, G. Sjoden, R. Porter, M. T. Athon, T. Tasdizen, V. Noel, S. M. Webb, A. Van Veelen, S. M. Hickam and C. Ly, *J. Nucl. Mater.*, 2024, **588**, 154779.
41 B. Morel and B. Duperret, *J. Fluor. Chem.*, 2009, **130**, 7–10.
42 K. J. Pastoor, R. S. Kemp, M. P. Jensen and J. C. Shafer, *Inorg. Chem.*, 2021, **60**, 8347–8367.
43 G. Sibbens, A. Moens and R. Eykens, *J. Radioanal. Nucl. Chem.*, 2015, **305**, 723–726.
44 H. Jang, J. Louis-Jean, B. Childs, K. Holliday, D. Reilly, M. Athon, K. Czerwinski, D. Hatchett and F. Poineau, *R. Soc. Open Sci.*, 2022, **9**, 211870.
45 J. McFarlane, P. Taylor, D. Holcomb and W. P. Poore, *Review of Hazards Associated with Molten Salt Reactor Fuel Processing Operations (No. ORNL/TM-2019/1195)*, Oak Ridge National Laboratory, Oak Ridge, TN, 2019.
46 J. J. Katz and E. Rabinowitch, *The chemistry of uranium*, 1951.
47 J. K. Dawson, R. W. M. D'Eye and A. E. Truswell, *J. Chem. Soc.*, 1954, 3922–3929.
48 A. Miskowiec, K. J. Pastoor, J. H. Christian, J. L. Niedziela, B. J. Foley, S. Isbill, A. E. Shields, L. L. Daemen, E. Novak, E. Nykwest, T. Spano, M. S. Wellons, M. Jensen and J. Shafer, *J. Phys. Chem. C*, 2021, **125**, 25007–25021.
49 J. H. Christian, C. A. Klug, M. Devore, E. Villa-Aleman, B. J. Foley, N. Groden, A. T. Baldwin and M. S. Wellons, *Dalton Trans.*, 2021, **50**, 2462–2471.
50 J. G. Tobin, A. M. Duffin, S.-W. Yu, R. Qiao, W. L. Yang, C. H. Booth and D. K. Shuh, *J. Vac. Sci. Technol., A*, 2017, **35**, E108.
51 C. A. Klug and J. B. Miller, *Solid State Nucl. Magn. Reson.*, 2018, **92**, 14–18.
52 S. P. Gabuda, L. G. Falaleeva and Y. V. Gagarinskii, *Phys. Status Solidi*, 1969, **33**, 435–438.
53 A. Miskowiec, A. E. Shields, J. L. Niedziela, Y. Cheng, P. Taylor, G. DelCul, R. Hunt, B. Spencer, J. Langford and D. Abernathy, *Phys. B*, 2019, **570**, 194–205.
54 E. Villa-Aleman and M. S. Wellons, *J. Raman Spectrosc.*, 2016, **47**, 865–870.
55 A. Y. Teterin, Y. A. Teterin, K. I. Maslakov, A. D. Panov, M. V. Ryzhkov and L. Vukcevic, *Phys. Rev. B: Condens. Matter Mater. Phys.*, 2006, **74**, 5101.
56 D. T. Hodul, *Spectrosc. Lett.*, 1983, **16**, 181–191.
57 C. Görller-Walrand, M. P. Gos and W. D'Olieslager, *Radiochim. Acta*, 1993, **62**, 55–60.
58 W. H. Zachariasen, *Acta Crystallogr.*, 1949, **2**, 388–390.
59 A. C. Larson, R. B. Roof Jr and D. T. Cromer, *Acta Crystallogr.*, 1964, **17**, 555–558.
60 T. K. Keenan and L. B. Asprey, *Inorg. Chem.*, 1969, **8**, 235–238.
61 J. Shankar, P. G. Khubchandani and V. M. Padmanabhan, *Anal. Chem.*, 1957, **210**, 1374.
62 B. Scheibe, J. Bruns, G. Heymann, M. Sachs, A. J. Karttunen, C. Pietzonka, S. I. Ivlev, H. Huppertz and F. Kraus, *Chem. – Eur. J.*, 2019, **25**, 7366–7374.
63 S. Kern, J. Hayward, S. Roberts, J. W. Richardson, F. J. Rotella, L. Soderholm, B. Cort, M. Tinkle, M. West, D. Hoisington and G. H. Lander, *J. Chem. Phys.*, 1994, **101**, 9333–9337.
64 A. Miskowiec, *Phys. Chem. Chem. Phys.*, 2018, **20**, 10384–10395.
65 J. Plaue, *Signatures of Chemical Process History in Uranium Oxides*, University of Nevada, Las Vegas, 2013.
66 K. J. Pastoor, A. J. Miskowiec, J. L. Niedziela, J. H. Christian, B. J. Foley, S. B. Isbill, A. E. Shields, A. M. Manjón-Sanz, E. C. Nykwest, T. L. Spano, M. S. Wellons, J. C. Shafer and M. P. Jensen, *J. Phys. Chem. C*, 2022, **126**, 13256–13267.
67 H. Jang and F. Poineau, *ACS Omega*, 2024, **9**, 26380–26387.
68 L. Wang, R. Zhao, C. Z. Wang, L. Y. Yuan, Z. J. Gu, C. L. Xiao, S. A. Wang, X. W. Wang, Y. L. Zhao, Z. F. Chai and W. Q. Shi, *Chem. – Eur. J.*, 2014, **20**, 12655–12662.
69 J. Louis-Jean, H. Jang, A. J. Swift and F. Poineau, *ACS Omega*, 2021, **6**, 26672–26679.